The Astrophysical Journal, 620:1118–1131, 2005 February 20

THE ACOUSTIC SHOWERGLASS. II. IMAGING ACTIVE REGION SUBPHOTOSPHERES

Charles Lindsey and D. C. Braun
Colorado Research Associates Division, NorthWest Research Associates, Inc., 3380 Mitchell Lane, Boulder, CO 80301;
clindsey@cora.nwra.com, dbraun@cora.nwra.com
Received 2004 July 10; accepted 2004 September 16

ABSTRACT

Seismic diagnostics of the shallow subphotospheres of strong active regions are substantially impacted by large amplitude and phase perturbations introduced by overlying surface magnetic fields. These function as an "acoustic showerglass" that impairs the coherence of acoustic waves impinging onto the solar surface from below, degrading images of subsurface anomalies derived by phase-coherent seismic reconstruction. In an independent study we have developed a rough proxy to characterize showerglass phase errors based on maps of the square magnitude of the vector magnetic field at the surface. In this study we apply the proxy to correct helioseismic observations of active region photospheres from the Michelson Doppler Imager aboard the *Solar and Heliospheric Observatory.* We apply phase-correlation seismic holography to the corrected observations to image the underlying 5–10 Mm subphotosphere. The corrected phase maps show no consistent evidence for sound-speed anomalies more than 5 Mm beneath a moderately large, isolated sunspot. Forward-modeling computations applied to simple models suggest sound-speed anomalies limited to approximately ± 250 m s^{-1} for depths from 5 to 10 Mm, averaged over the horizontal extent of the sunspot. For complex active regions, uncertainties are considerably greater. However, results of this study suggest that more careful modeling of the acoustic showerglass will lead to substantially improved seismic diagnostics of active region subphotospheres. Detailed hydromechanical computations of acoustics models of active region photospheres and subphotospheres are needed to facilitate the interpretation of showerglass-corrected holographic signatures.

Subject headings: Sun: activity — Sun: helioseismology — Sun: magnetic fields — Sun: oscillations — sunspots

1. INTRODUCTION

A subject of major interest in local helioseismology has been the structure and dynamics of the relatively shallow subphotospheres of active regions (e.g., Braun et al. 1992a; Braun 1995; Fan et al. 1995; Duvall et al. 1996; Kosovichev 1996; Kosovichev et al. 2000). In principle, acoustic waves allow us to look beneath the solar surface to view subphotospheric refractors and Doppler scatterers. This is one of the prospective applications of phase-correlation seismic holography (Lindsey & Braun 2000; Braun & Lindsey 2000) and time-distance tomography (Duvall et al. 1996; Kosovichev 1996; Kosovichev et al. 2000). The major obstacles for seismic diagnostics of the shallow subphotospheres of active regions, as we understand it, are the large amplitude and phase perturbations the magnetic photosphere introduces to the acoustic signatures of waves arriving from the underlying solar interior.

This study makes frequent reference to two recent papers, Lindsey & Braun (2004) and Lindsey & Braun (2005), to which we refer as LB04 and Paper I, respectively. LB04 develops the basic practical elements of computational seismic holography of the shallow subphotosphere. Paper I undertakes a general appraisal of the acoustic showerglass based on comparisons of acoustic amplitudes, ψ, in magnetic photospheres with holographic projections, $H_{\pm}$, of waves arriving at or leaving the active region, for a first-order appraisal of showerglass perturbations. Using the statistics of these "local control correlations," Paper I developed a magnetic proxy to represent the showerglass perturbations as a function of the square magnetic field, B^2.

In this study, we use the magnetic proxy to implement an optical correction of the showerglass that considerably improves holographic imaging of the underlying subphotosphere. We apply standard phase-correlation holography (Lindsey & Braun 2000) to helioseismic observations of an active region from the Michelson Doppler Imager (MDI) aboard the *Solar and Heliospheric Observatory* (*SOHO*) to image the active region subphotosphere. Paper I explains the empirical basis of the magnetic proxy and discusses applications in modeling of the upper megameter of magnetic subphotospheres. This study concentrates on imaging the underlying 5–10 Mm subphotosphere.

2. BASIC PRINCIPLES

2.1. *The Born Approximation*

Holographic diagnostics of a local acoustic anomaly are essentially based on how the anomaly shifts the phase of acoustic radiation that encounters it, as compared with the phase with which the radiation would have arrived at the surface if the anomaly had been absent. If the acoustic radiation arrives at the solar surface with a scrambled phase because it has passed through a swarm of other intervening anomalies, then the analyst is confronted with the basic problem of trying to "see" through a cloud or fog bank. For purposes of seismic diagnostics of active region subphotospheres, we say that the Born approximation is satisfied if a substantial fraction of acoustic radiation propagates from the supposed location of the anomaly of interest to the solar surface without undergoing further significant scattering. This is generally secured if the intervening phase perturbations are appropriately small ($\ll 1$ rad) for a significant portion of the radiation.

The function of a showerglass is to introduce relatively large, stochastic phase variations such that modeling based on the Born approximation is prohibitive. In the practical realm,

it appears that modeling of any sort is prohibitive when the Born approximation is thoroughly violated in stochastic terms. We have generally been forced to treat the problem of interpreting an optical image reconstructed from radiation that has passed through a well-designed showerglass as a hopeless proposition. A common recourse when this is the case is to remove or flatten the showerglass. As a familiar electromagnetic example, this is the basic function of windshield wipers. It has major extensions in recent techniques in adaptive optics. The practicality of adaptive optics is based largely on the showerglass phase errors being introduced in a relatively thin layer. The basic principle is to assess the phase errors as close as possible to where they are introduced and remove them in order to procure a representation of the amplitude that would characterize the radiation in the absence of the showerglass.

2.2. *Phase-Correlation Seismic Holography*

In this study we use phase-correlation seismic holography in the lateral vantage to image an active region subphotosphere with and without a showerglass correction. The computational basis of phase-correlation holography is maps of the correlation,

$$C^{\mathcal{LR}}(\boldsymbol{r},\ z) \equiv \langle H_+^{\mathcal{L}}(\boldsymbol{r},\ z,\ \nu) H_-^{\mathcal{R}*}(\boldsymbol{r},\ z,\ \nu)\rangle_{\Delta\nu}, \tag{1}$$

where the complex fields $H_\pm^{\mathcal{P}}(z)$ represent holographic projections,

$$H_\pm^{\mathcal{P}}(z) = U_\pm^{\mathcal{P}}(z)\psi, \tag{2}$$

of the surface acoustic field, represented by a complex function, $\psi(\boldsymbol{r},\ \nu)$, of surface location, $\boldsymbol{r}$, and frequency, ν, over a surface pupil, $\mathcal{P}$. The operator $U_-^{\mathcal{P}}(z)$ applied to ψ progresses ψ in the pupil forward in time to the submerged focal plane at depth z. The operator $U_+^{\mathcal{P}}(z)$ similarly regresses ψ back in time to the same focal plane. We call the operators $U_\pm(z)$ "holographic progressions." We call the image field, $H_\pm$, of $U_\pm(z)$ applied to ψ a "holographic projection" of ψ. For a more detailed explanation of this formalism we refer to Paper I. For still further details and examples of the computational procedures that accomplish the progressions $U_\pm^{\mathcal{P}}(z)$, we refer the reader to Lindsey & Braun (2000).

2.3. *The Magnetic Proxy*

The magnetic proxy attempts to correct the surface acoustic field, $\psi(\boldsymbol{r},\ \nu)$, simply by multiplying it by a complex amplitude, $\Lambda(B^2)$, where B is the magnitude, $|\boldsymbol{B}|$, of the magnetic field vector, $\boldsymbol{B}$, at $\boldsymbol{r}$. The magnetic field vector, $\boldsymbol{B}$, is reconstructed from a line-of-sight MDI magnetogram during the acoustic observations under the assumption that $\boldsymbol{B}$ above the solar surface is the gradient of some potential,

$$\boldsymbol{B} = \nabla\Phi. \tag{3}$$

Because the phase shift between $\psi(\boldsymbol{r},\ \nu)$ and $H_-^{\mathcal{P}}(\boldsymbol{r},\ \nu)$ differs considerably from that between $\psi(\boldsymbol{r},\ \nu)$ and $H_+^{\mathcal{P}}(\boldsymbol{r},\ \nu)$, the proxy applies separate corrections,

$$\psi_\pm = \Lambda_\pm(B^2)\psi, \tag{4}$$

for ingression and egression computations. The holographic projections, $H_\pm^{\mathcal{P}}$, are then computed by applying operators $U_\pm^{\mathcal{P}}(z)$ to $\psi_\pm$:

$$H_\pm^{\mathcal{P}}(z) = U_\pm^{\mathcal{P}}(z)\psi_\pm. \tag{5}$$

In point of fact, the proxy developed in Paper I has significant limitations:

1. It does not entirely correct for suppression of $|\psi|$ by the magnetic photosphere.
2. It does not take into account the effect of the inclination of $\boldsymbol{B}$, which Paper I found to be important. This leaves residual phase errors that we estimate to be of the order of 0.2 rad. The residual phase errors do considerably less damage to the coherence of ψ than the uncorrected showerglass but can leave significant artifacts to compete with the relatively weak signatures expected from submerged scatterers.

For further details as to how the complex functions $\Lambda_\pm(B^2)$ were derived and their limitations, we refer to Paper I.

In practice, it is frequently useful to fashion a modification of the initial proxy for various purposes. All of the variations applied in this study are conveniently expressed in terms of the original proxy stated in Paper I. In this study we refer to the original proxy by the notation "$\Lambda_{0\pm}(B^2)$."

3. HOLOGRAPHY THROUGH THE SHOWERGLASS

We begin this section with a review of holographic projections of MDI Doppler observations directly through the acoustic showerglass and into the active region subphotosphere with no correction for the showerglass. We compute the acoustic egressions and ingressions in the lateral vantage, as illustrated in Figure 1*b* of LB04. In this study we examine only the signatures of refractors, not flows.

Figure 1 shows phase maps for AR 8179 with acoustic progressions computed over two different combinations of pupils. Both computations are integrated over a 10.6 hr period beginning on 1998 March 15 at 11:00 UT. The left column below the top row shows gray-scale images of $\phi^0 \equiv \arg C^{\mathcal{OO}}$, for which the acoustic progressions were computed over a simple, self-conjugate annular pupil, $\mathcal{O}$, the same for both ingression and egression, as in Figure 13 of LB04. The right column shows the symmetric phase signature,

$$\phi^S = \frac{1}{2}(\arg C^{\mathcal{LR}} + \arg C^{\mathcal{RL}}), \tag{6}$$

for which the ingression and egression computations were integrated over separate, mutually conjugate pupils, $\mathcal{L}$ and $\mathcal{R}$. These are quarter-annular regions centered on the vertical projection of the submerged focal point to the solar surface such that the focal point is illuminated by ray paths passing through it with angles in the range $\pm 45^\circ$ from horizontal (see Fig. 1*b* of Paper I). The quarter-annular regions are mutually opposite each other with respect to the focal point and separated in the east-west direction ($\mathcal{L}$-$\mathcal{R}$). The term $C^{\mathcal{LR}}$ correlates the ingression computed over the pupil $\mathcal{L}$ with the egression computed over $\mathcal{R}$. The pupils are swapped to render the reverse, $C^{\mathcal{RL}}$. The symmetric phase, ϕ^S, is therefore invariant with respect to east-west reflection of the pupil configuration about the focal point. In the case of identical pupils, $\mathcal{L} = \mathcal{R} = \mathcal{O}$ (Fig. 1, *left column*), ϕ^S devolves to ϕ^0, to which we therefore likewise apply the term "symmetric phase."

We now proceed with a brief review of the major points cited by LB04 regarding subphotospheric projections of acoustic fields in magnetic photospheres uncorrected for showerglass perturbations.

3.1. *The Large-Scale Diffuse Signature*

As LB04 conclude, the major component of ϕ^S for focal planes beneath 5 Mm is a diffuse negative signature. This is the

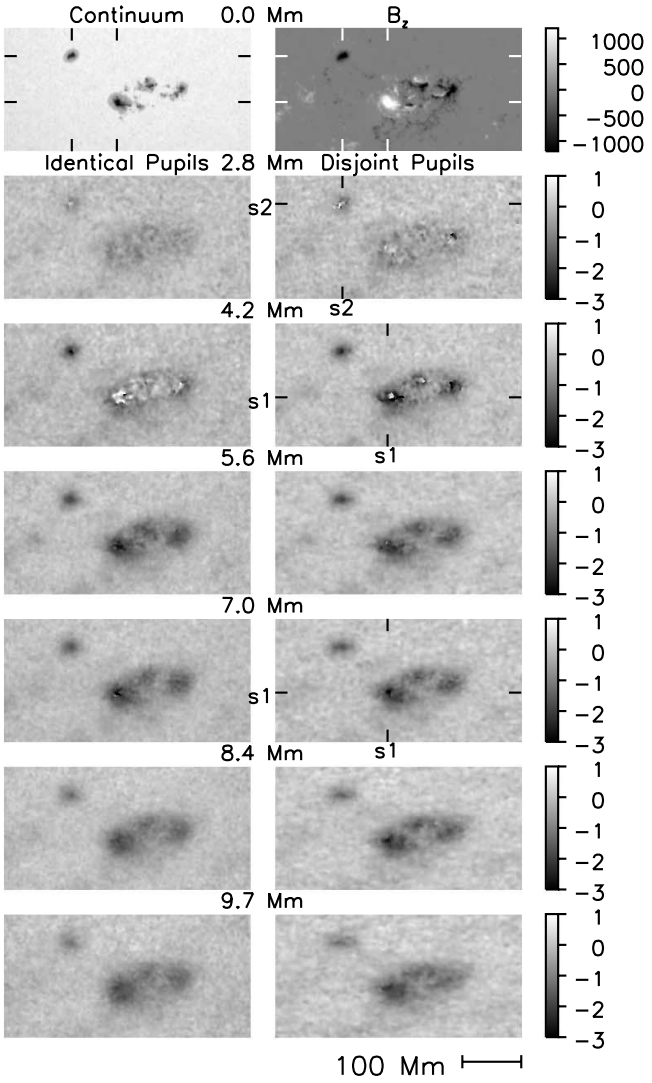

FIG. 1.—Gray-scale images of the symmetric phase, ϕ^S, of the egression-ingression correlation for focal planes over the depth range 2.8–9.7 Mm. The left column shows ϕ^S for egression and ingression computations integrated over identical annular pupils. The right column shows ϕ^S for egression and ingression computations integrated over separate quarter-annular pupils opposite each other with respect to the focal point. Depths are indicated above the center of each row. The acoustic progressions were integrated over a time interval of 10.6 hr beginning at 11:00 UT on 1998 March 15. Vertical and horizontal fiducials labeled "s1" in the right 7 and 4.2 Mm frames locate sunspot 1, at the east edge of AR 8179. Vertical and horizontal fiducials labeled "s2" in the right 2.8 Mm frame locate sunspot 2, the isolated monopolar spot ~100 Mm northeast of sunspot 1 that is also designated AR 8178.

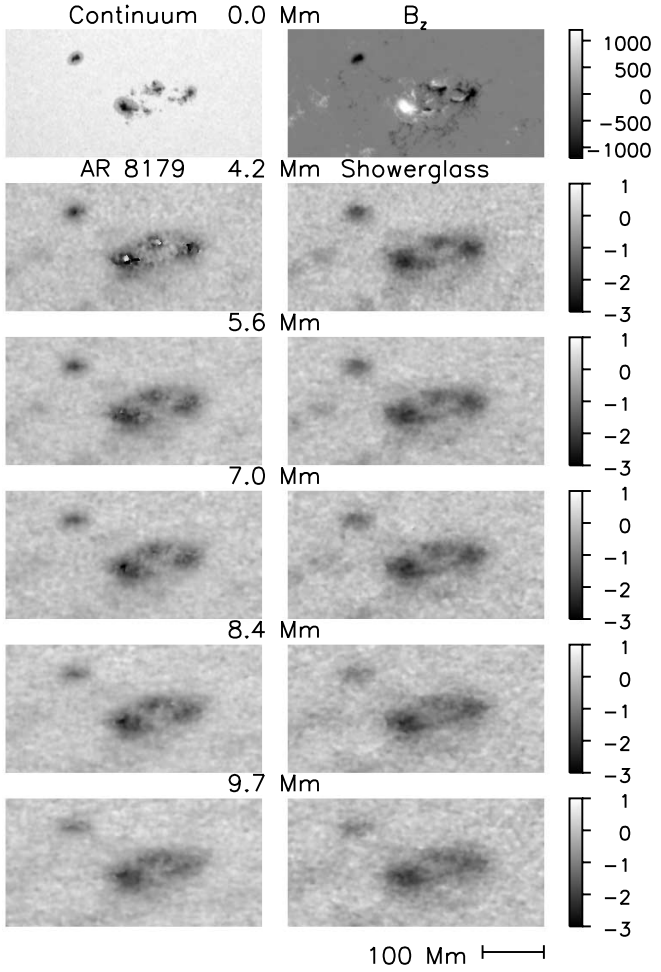

FIG. 2.—Gray-scale images of the symmetric phase, ϕ^S, of the egression-ingression correlation for AR 8179 (*left column*) compared with a control computation (*right column*). The phase correlations represented in the left column were computed with quarter-annular pupils and are taken from the right column of Fig. 1. The control computations were accomplished by applying the same egression and ingression computations to a region of quiet Sun with the showerglass phase correction applied in reverse to represent a superficial anomaly, i.e., a showerglass with no underlying anomalies. No correction for the modulus was applied to the quiet-Sun computations.

holographic facsimile of an important scattering signature discovered by Braun et al. (1992b) and a major topic of succeeding work by Braun (1995, 1997), Fan et al. (1995), Duvall et al. (1996), Hindman et al. (2000), Lindsey & Braun (2000), and many others. Fan et al. (1995) presented strong evidence that the acoustic anomaly that gives rise to the active region phase is predominantly superficial. This explains the gradual defocusing of the signatures in Figure 1 as the focal plane submerges.

Figure 2 compares the phase signatures of AR 8179 (*left column*) with holographic computations of a quiet-Sun acoustic field to which a showerglass phase perturbation representing AR 8179 has been artificially applied (*right column*). The left column of Figure 2 is a reproduction of the right column of Figure 1, representing computations over mutually conjugate quarter-annular pupils. The quiet-Sun computations (Fig. 2, *right column*) were made over identical quarter-annular pupils.

The phase maps shown in the right column of Figure 2 serve as a control computation to represent the subphotospheric artifact of an active region with only a showerglass and no underlying acoustic anomaly. In this control computation only a phase perturbation,

$$\Lambda_{\mathrm{QS}\pm} = \exp\left(-i\alpha \arg \Lambda_{0\pm}\right), \tag{7}$$

was applied to the observations, since an amplitude adjustment to correct suppression of the acoustic field in the quiet Sun would be superfluous. A value of 0.8 was chosen for α to optimize the similarity between the control computations and the phase signature of the active region itself for the greatest depths. The reason for the minus sign in front of the i is that the purpose of $\Lambda_{\mathrm{QS}\pm}$ is to simulate the showerglass rather than to correct it. The subunity value for α in the control computation recognizes that the statistics derived in the initial proxy were based on showerglass measurements that allowed some contamination of the supposedly quiet pupil with magnetic

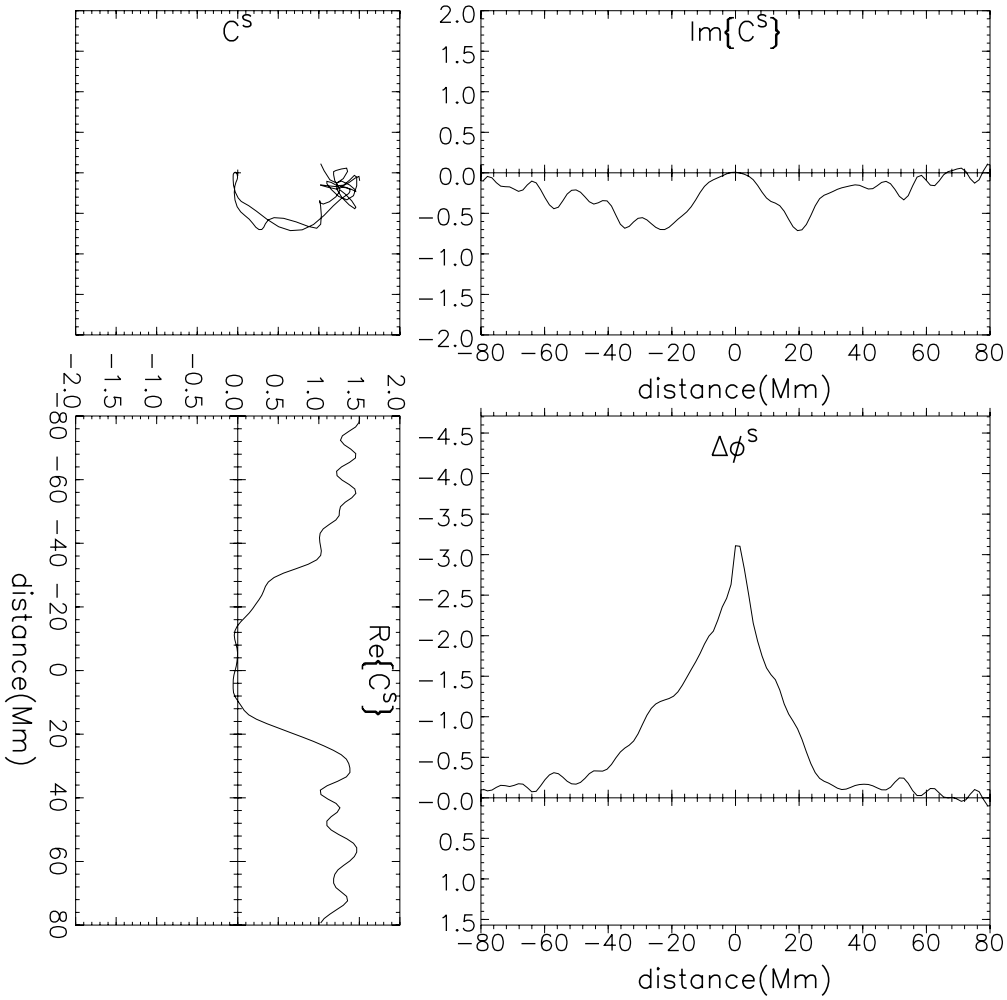

FIG. 3.—Diagnostic plots of the symmetric correlation, C^S, from south to north through sunspot 1 at a depth of 7 Mm and symmetric phase, ϕ^S, uncorrected for the showerglass (see vertical fiducial labeled "s1" in right 7 Mm frame of Fig. 1). The abscissae in the plots of ReC^S (*lower left*), ImC^S (*upper right*), and $\Delta\phi^S$ (*lower right*) are referenced to zero at the center of sunspot 1 (see horizontal fiducial labeled "s1" in the right 7 Mm frame of Fig. 1).

photospheres, resulting in a general overestimate of the phase shifts introduced by the showerglass (see discussion of Figs. 4 and 5 in § 3.1 of Paper I).

The predominant negativity of ϕ^S in Figures 1 and 2 is equivalent to a reduction,

$$\Delta t = \frac{\phi^S}{\omega}, \tag{8}$$

in the phase travel time, t, indicated by the signature. Thus, the deeper focal planes in Figures 1 and 2 appear to be predominated by a signature that is closely equivalent to that due to a superficially introduced phase shift. We call the acoustic anomaly that causes this phase perturbation the "acoustic Wilson depression" (see § 5.1).

3.2. *The Islands*

As mentioned in LB04, the large-scale diffuse signatures in Figure 1 are punctuated by sharply defined "islands" of differing phase marking the regions of strongest magnetic field. Examples are the large sunspot at the east end of AR 8179, which we call "sunspot 1," and the isolated sunspot approximately 100 Mm northeast of AR 8179, which NOAA identifies as AR 8178 and we call "sunspot 2." In the case of sunspot 2 the island signature appears only at 2.8 Mm. For sunspot 1 the island signature is seen at 7.0 Mm, in both the left and right columns of Figure 1.

Figure 3 shows diagnostic plots of the symmetric correlation,

$$C^S \equiv \frac{1}{2}(C^{\mathcal{LR}} + C^{\mathcal{RL}}), \tag{9}$$

from south to north through sunspot 1 along the vertical trajectory marked by the fiducial labeled "s1" at the bottom of the 7.0 Mm frame in the right column of Figure 1 showing the phase of the quarter-annular correlation. The horizontal fiducial, likewise labeled "s1" at the left side of the same frame, marks the location of sunspot 1 along the north-south trajectory.

Figure 3 shows that the compactness suggested by the sharp phase signature in Figure 1 is largely illusory. As the point of reference along s1 proceeds north, the locus of C^S in the complex plane (*top left*) winds clockwise, sliding gently into the origin approaching sunspot 1. The modulus, $|C^S|$, undergoes a crater-like drop over a distance of some 80 Mm. The sharp inflection in ϕ^S (*lower right*) occurs in a relatively narrow region in which C^S is so close to zero that a small accidental variation, ΔC, can manifest an inordinate variation in the phase, ϕ^S.

The islands invariably occur when the modulus of the correlations of which the phases are arguments are severely suppressed. Figures 4 and 5 show diagnostic plots of sunspots 1

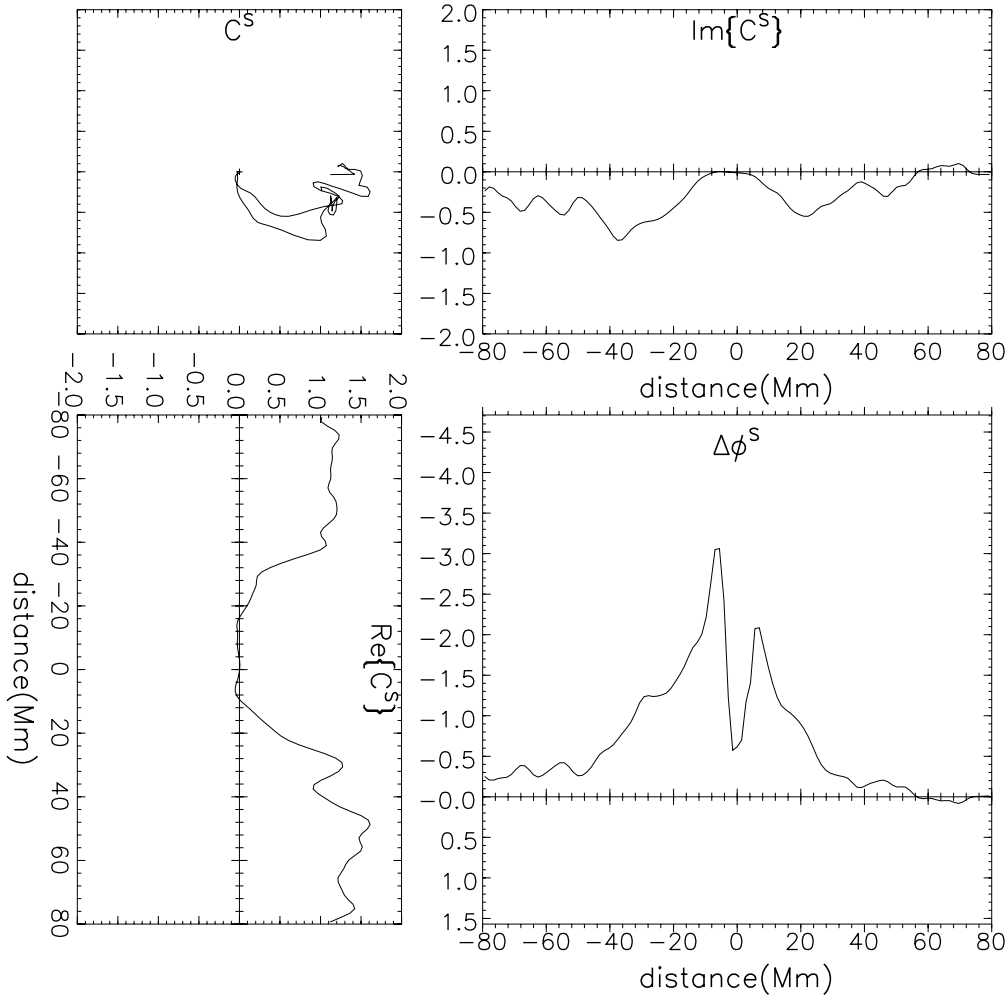

FIG. 4.—Diagnostic plots of the symmetric correlation, C^S, and symmetric phase, ϕ^S, from south to north through sunspot 1 at a depth of 4.2 Mm, uncorrected for the showerglass (see Fig. 1). The configuration for these is the same as for Fig. 3, with the abscissae in the plots of ReC^S (*lower left*), ImC^S (*upper right*), and $\Delta\phi^S$ (*lower right*) referenced to zero at the center of sunspot 1 (see horizontal fiducial labeled "s1" in the right 4.2 Mm frame of Fig. 1).

and 2 along shallower focal planes. Figure 4 shows south-to-north diagnostic plots of C^S through sunspot 1 in the right column of Figure 1 at 4.2 Mm (see fiducial labeled "s1" in right 4.2 Mm frame of Fig. 1). Figure 5 shows a similar plot through sunspot 2 at 2.8 Mm (see fiducial labeled "s2" in right 2.8 Mm frame in Fig. 1). Beneath 5.6 Mm, the phases of the island signatures tend to be positive.

The severe suppression of $|C^S|$ that invariably accompanies the island signatures can be attributed to at least three factors:

1. The general suppression of the acoustic signature in magnetic photospheres.
2. The loss of coherence due to phase errors introduced by the showerglass.
3. Various instrumental factors that concern Doppler measurements in sunspots, probably including considerations of line formation in sunspot photospheres and noise introduced by scattered light.

The islands are generally stronger in the full-annular correlations than in the quarter-annular correlations. This leads LB04 to suggest that the ghost signatures have something to do with the island signatures.

In principle, the island signatures could be partly the result of strong compact scatterers at the depth of the focal plane. However, without measures to correct the strong modulus and phase perturbations introduced by the showerglass, evidence for significant submerged scatterers must be regarded as insubstantial. We return to a discussion of the island signatures in § 5.2. For the remainder of this study, we regard acoustic anomalies down to a depth of 4.2 Mm as part of the showerglass.

4. CORRECTING THE SHOWERGLASS

For purposes of correcting the showerglass, we shift our attention to holographic computations over quarter-annular pupils over focal planes beneath the showerglass, i.e., at 5.6 Mm and below. Under the Born approximation, the showerglass could be credibly corrected for an actual magnetic region by subtracting the right column of Figure 1 from the left column. In fact, the strong perturbations introduced by the showerglass are sufficient to degrade the phase-coherent image that would remain even after the signature of the showerglass itself was accurately subtracted.

The alternative approach we fashion for this study is a computational adaptation of the familiar optical function of windshield wipers: we apply the magnetic proxy developed in Paper I directly to the surface acoustic field to reverse the showerglass phase errors. The proxy, $\Lambda_{\pm}$, that we apply here, like $\Lambda_{0\pm}$ prescribed in Paper I, also amplifies the acoustic field in the magnetic region, partially correcting for the significant suppression of the acoustic signature in the magnetic photosphere

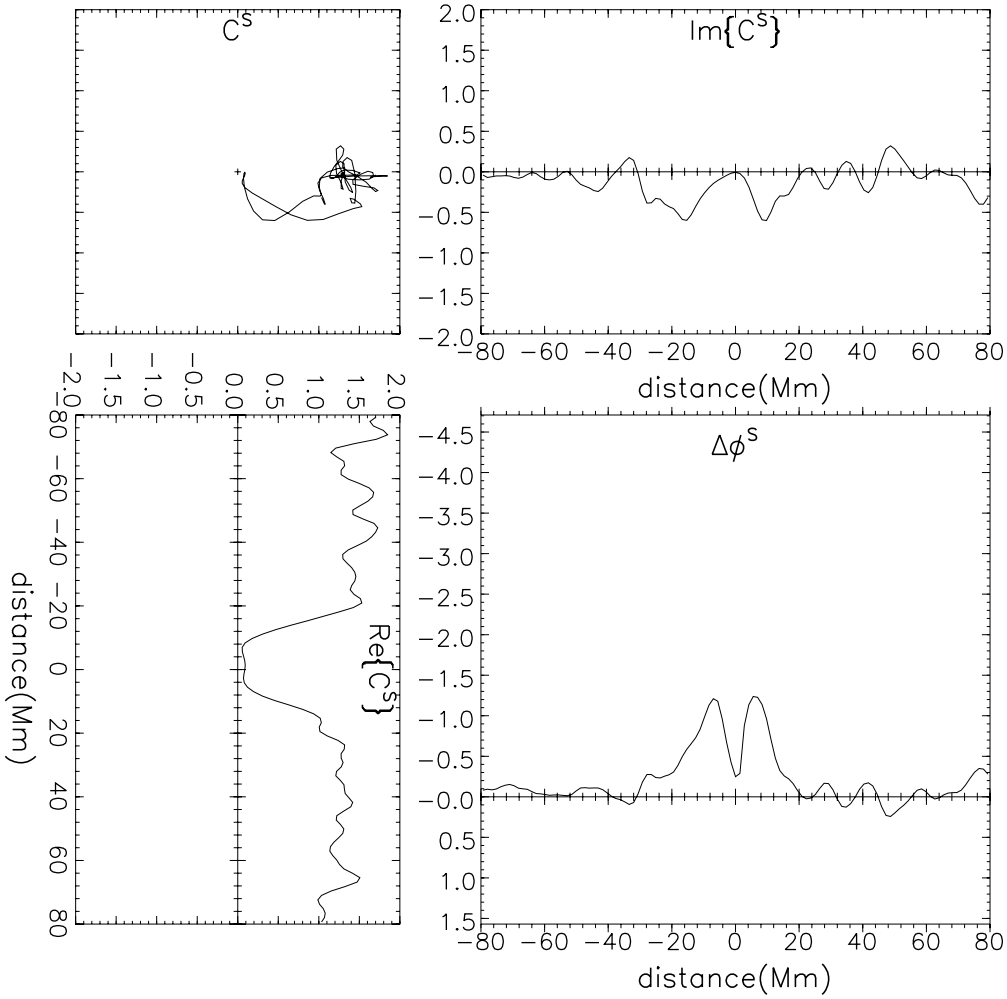

FIG. 5.—Diagnostic plots of the symmetric correlation, C^S, and symmetric phase, ϕ^S, from south to north through sunspot 2 at a depth of 2.8 Mm uncorrected for the showerglass. The configuration for these is the same as for Figs. 3 and 4, with the abscissae in the plots of ReC^S (*lower left*), ImC^S (*upper right*), and $\Delta\phi^S$ (*lower right*) referenced to zero at the center of sunspot 2 (see fiducial labeled "s2" in the right 2.8 Mm frame of Fig. 1).

($|\Lambda_\pm(B^2)| = |\Lambda_{0\pm}(B^2)| > 1$ in strong magnetic fields). However, $\Lambda_\pm$ is different from $\Lambda_{0\pm}$ in that it retains the factor $\alpha = 0.8$ appearing in equation (7). Thus,

$$\Lambda_\pm = |\Lambda_{0\pm}| \exp(+i\alpha \arg \Lambda_{0\pm}). \quad (10)$$

Figure 6 shows ϕ^S for AR 8179 corrected for the showerglass according to this proxy, applied as equations (4) and (5) prescribe. Once the respective corrections are applied to the observations, the acoustic ingressions and egressions are computed therefrom over separate quarter-annular pupils, as in the right column of Figure 1. The left column of Figure 6 shows the phase, ϕ^S, on a gray scale whose range is similar to that of Figure 1. The right column shows the same at 2.5 times the contrast applied to the left.

Figure 7 shows south-to-north diagnostic plots of C^S through sunspot 1 at 7 Mm corrected for the showerglass (see fiducial labeled "s1" in the right 7 Mm frame of Fig. 6). The decrease in $|C^S|$ now occurs over a somewhat narrower south-north range than it did for the uncorrected computation. Nevertheless, C^S slides directly into the origin at the location of the sunspot, and the phase, ϕ^S, shows a somewhat stochastic signature at the center of the sunspot that is not characteristic of C^S itself.

Figure 8 shows a south-to-north diagnostic plot of C^S through sunspot 2 at 7 Mm corrected for the showerglass (see fiducial labeled "s2" in the right 7 Mm frame of Fig. 6). In this case, $|C^S|$ is significantly positive 7 Mm directly beneath the sunspot. A weak signature is suggested in Figure 6 at 5.6 Mm and perhaps 7 Mm. However, the signs of these signatures are indefinite and the significance questionable.

Figure 9 shows ϕ^S for AR 8179 integrated over two consecutive 10.6 hr periods. The left column, labeled "16:20 UT," shows ϕ^S for AR 8179 integrated over a 10.6 hr period beginning at 11:00 UT. This is identical to the right column of Figure 6. The right column, labeled "27:00 UT," shows ϕ^S for AR 8179 integrated over the 10.6 hr period beginning at 21:40 UT, directly after the end of the first period. The signature of sunspot 2 remains inconspicuous below 5 Mm. However, differences between these two maps are conspicuous in the case of AR 8179. A thin region of relatively negative phase appears along the horizontal axis of AR 8179 in the 27:00 UT interval. Much of this signature lies in the penumbra and umbra of sunspot 1. However, it extends $\sim$25 Mm outside the penumbral boundary on the west side. Figure 10 shows a south-to-north diagnostic plot along the fiducial labeled *e* in Figure 9. It shows a signature of $\sim$0.5 rad over a north-south width of $\sim$8 Mm. This suggests a travel time reduction of up to 16 s when the anomaly is centered on the focal point. The nominal travel time through an anomaly 8 Mm across at a maximum depth of 8.4 Mm is 170 s, of which 16 s is approximately 10%.

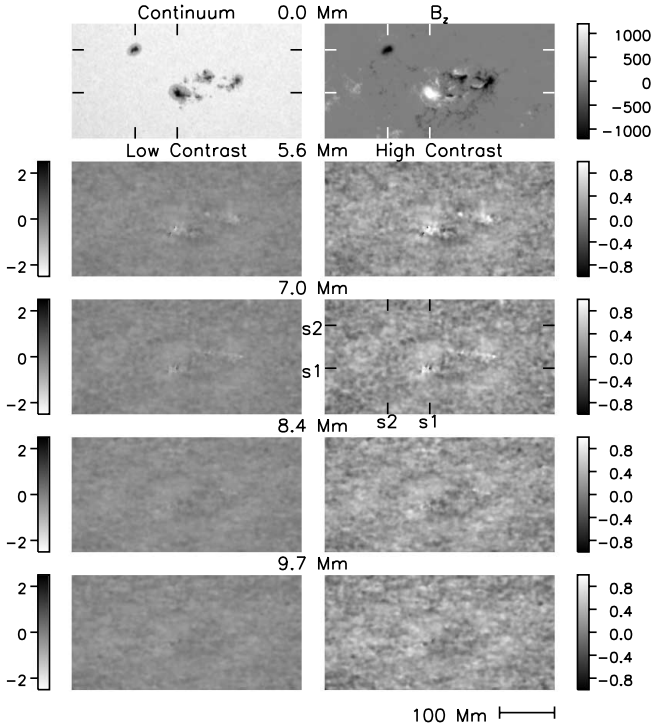

FIG. 6.—Gray-scale images of the symmetric phase, ϕ^S, of the egression-ingression correlation for AR 8179 (*left column*) of helioseismic observations corrected for the showerglass as represented by eq. (13) in Paper I. The left column shows ϕ^S on gray scales similar to those of Figs. 1 and 2 for focal plane depths in the range 5.6–9.7 Mm. The right column shows the same but with contrast enhanced by a factor of 2.5. As in Fig. 1, the acoustic progressions were integrated over a time interval of 10.6 hr beginning at 11:00 UT on 1998 March 15. Fiducials labeled "s1" and "s2" in the right 7 Mm frame locate sunspots 1 and 2, as in Fig. 1.

This would suggest a sound-speed enhancement, $\Delta c/c \sim 0.1$, or a temperature perturbation of the order of $\Delta T/T \sim 0.2$, highly unrealistic according to our present understanding.

A careful comparison of the roughly concurrent magnetograms (Fig. 9, *top row*) shows that a substantial amount of magnetic flux has emerged into the pupils of the computations for focal points in region *e* in the period between 16:20 and 27:00 UT. The magnetogram on which the showerglass correction is based is a single snapshot applied to the entire 10.6 hr acoustic time series. A significant change in the showerglass during this interval opens the possibility of a showerglass signature that escapes the correction. A crude test of this proposition is accomplished by running comparative showerglass-corrected computations with the magnetograms swapped. The result, shown in Figure 11, reinforces the foregoing concern. The differences between Figures 9 and 11 suggest the range of subphotospheric artifacts that can be projected by residual showerglass errors. These are quite imposing. The errors introduced by swapping the showerglass corrections give rise to conspicuous artifacts in the neighborhood that are more than a match for the largest signatures visible in Figure 9.

5. DISCUSSION

5.1. *The Acoustic Wilson Depression*

The phases, ϕ^0 and ϕ^S, of the egression-ingression correlations (see Figs. 1 and 2) show comparably negative signatures suggesting similarly reduced travel times that defocus as the focal plane submerges. These are roughly consistent with the travel time deficits suggested by the local control correlations, $\arg C_{\mathrm{LC}\pm}$, computed in Paper I, indicating similarly reduced one-way travel times both to and from the magnetic photosphere. While it is probable that a physical depression of the magnetic photosphere contributes to the acoustic signature, the mechanism must be more complicated than this alone. In any case, the substantial defocusing of the signature as the focal plane submerges suggests a subphotospheric anomaly that is predominantly superficial. This proposition is reinforced by significant similarities between the left and right columns in Figure 2, which compare the phase-correlation signature of AR 8179 with control computations representing a superficial anomaly. As in LB04 and Paper I, in this study we generalize the term "acoustic Wilson depression" to include any superficial mechanism, or anomaly based thereon, that contributes to the large-scale, diffuse signatures in ϕ^0 and ϕ^S, whether or not it is based entirely on a literal physical depression of the local photosphere.

5.2. *The Islands*

The "penumbral phase anomaly," shown by the "local ingression control correlation" (see §§ 3.1 and 4.3 of Paper I), shows a feature faintly similar to the character of the island signatures in shallow focal planes. This is the tendency for the phase of the correlation to relax to a significantly lesser value in the umbrae of sunspots. However, these signatures are much weaker and smoother than the islands. More important, the moduli of the correlations do not nearly vanish even beneath the strongest magnetic fields. Like the penumbral phase anomaly, the islands invite the interpretation of umbral subphotospheres as particularly cool (i.e., having a reduced sound speed), possibly as represented by the models of Kosovichev et al. (2000).

In § 3.2, we briefly mentioned considerations relating the ghost signatures, discussed in §§ 5.7 and 7.3 of LB04, to the islands seen in Figures 1 and 2 of this paper. The involvement of the ghosts is supported by several considerations. The island signatures are considerably weaker when the pupils of the ingression and egression computations are disjoint than when they are identical, as seen in Figure 1. This is particularly characteristic of the ghost signatures. In the quiet Sun the ghosts are largely eliminated when the acoustic projections are computed over separate, disjoint pupils that are radially extensive and well separated (see § 7.3 of LB04). For separate, disjoint pupils the ghost is the diffuse signature of acoustic radiation that is traveling in the direction opposite to that in which the acoustic projections are focused. In the quiet Sun these ghosts, while quite spread out, are predominately projected to different, nonoverlapping regions of the focal plane when the pupils are well separated. As a result, their correlations, while noisy, are systematically almost null.

According to our current understanding, large phase perturbations by the showerglass may deflect acoustic radiation that is traveling in the wrong direction into the wrong pupil to revive the ghost, even while it degrades the correlation for acoustic radiation due to waves travelling in the proper direction. The loss of coherence due to the showerglass contributes to the reduction in $|C^{\mathcal{LR}}|$ evident in Figures 3–5. The additional suppression of acoustic emission from strong magnetic regions further exacerbates contamination of ingression computations by the much stronger flux of waves traveling in the wrong direction.

As we currently understand them, time-distance correlation measurements in general are susceptible to interference by ghosts to various degrees. The Doppler observations by themselves do not contain the information to discriminate the direction of propagation between any two points, *A* and *B* (or between a point and a thin surrounding annulus). As a result, acoustic

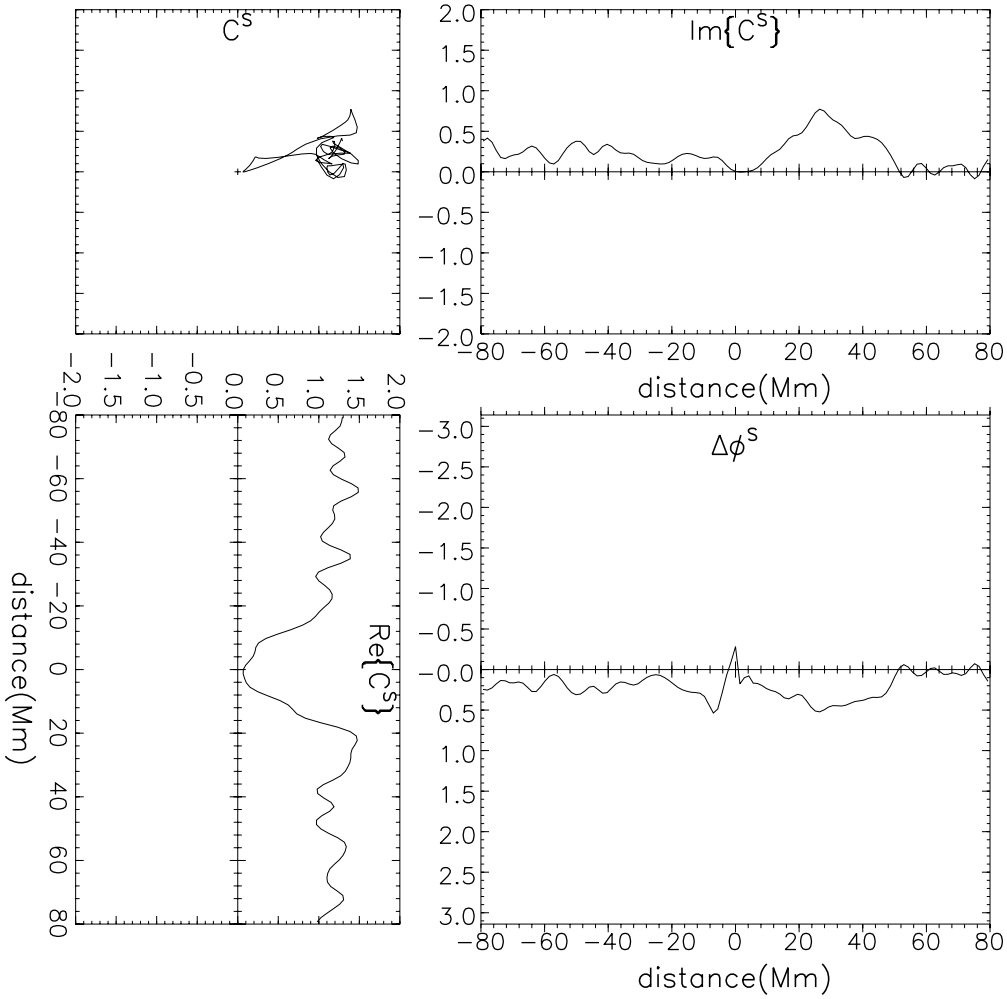

FIG. 7.—Diagnostic plots of the showerglass-corrected symmetric correlation, C^S, and symmetric phase, ϕ^S, from south to north through sunspot 1 at a depth of 7 Mm. The configuration for these is the same as for Fig. 3, with zero referenced to the center of sunspot 1 (see fiducial labeled "s1" in the right 7 Mm frame of Fig. 6).

cross-correlations, C, between A and B generally include at least two components: (1) a signature delayed by a positive travel time, T, as a result of acoustic disturbances beginning at or near A and skipping beneath the surface to arrive at B some time later, and (2) a signature delayed by a negative time, $-T$, as a result of the time reverse, i.e., acoustic disturbances beginning at or near B and skipping to A. Given a spectrum of limited bandwidth, $\Delta\nu$, these signatures must be temporally extensive, spanning a characteristic time of $1/\Delta\nu$ or greater. For optical paths confined to relatively shallow depths, z, such that $2T$ becomes of the order of $1/\Delta\nu$ or less, the sidelobes of the respective positively and negatively delayed temporal cross-correlation signatures extend clear across the origin, thereby interfering with each other to some degree. In the case of holographic projections over pupils that are radially extensive, waves traveling in the wrong direction to and from a radially extensive pupil project a ghost that is significantly out of focus. However, for pupils of lesser radial extent, focus becomes insensitive to travel direction. When the range of travel times from the inner to the outer radii of the pupil is of the order of $1/\nu$ or less, the ghost is likely to be imposing. We refer to §§ 5.7 and 7.3 in LB04 for further elaboration on considerations relating to the ghost signatures.

Careful modeling is needed to procure a quantitative assessment of the contribution of the ghost signatures to the phase-correlation maps in the showerglass subphotosphere. This is the subject of a computational study currently being initiated.

5.3. *The Extent of the Cool Sunspot Subphotosphere*

Figure 12 shows plots of the phase signatures of sunspots 1 and 2 in ϕ^S taken from Figure 1, with phase signatures estimated from a selection of simple sunspot models for which C^S was computed at a single frequency, 5 mHz. The sunspot models are represented by anomalies that are horizontally uniform inside a cylinder whose radius is 10 Mm. The acoustic projections through the model anomalies were computed along the axis of the cylinder under the eikonal approximation, taking advantage of cylindrical symmetry for sorely needed computational economy. No account was taken of acoustic suppression of the sunspot photosphere nor of acoustic radiation propagating in the wrong direction to reproduce the ghost signatures. These are greatly simplified facsimiles of detailed, three-dimensional, hydromagnetic forward-modeling computations we are planning for large parallel processors. The model computations presented in Figure 12 are therefore susceptible to a variety of uncertainties that will be addressed much more adequately by the more detailed hydromagnetic computations being planned.

The solid curve in Figure 12 shows the phase signatures for the eikonal computations applied to a model anomaly whose

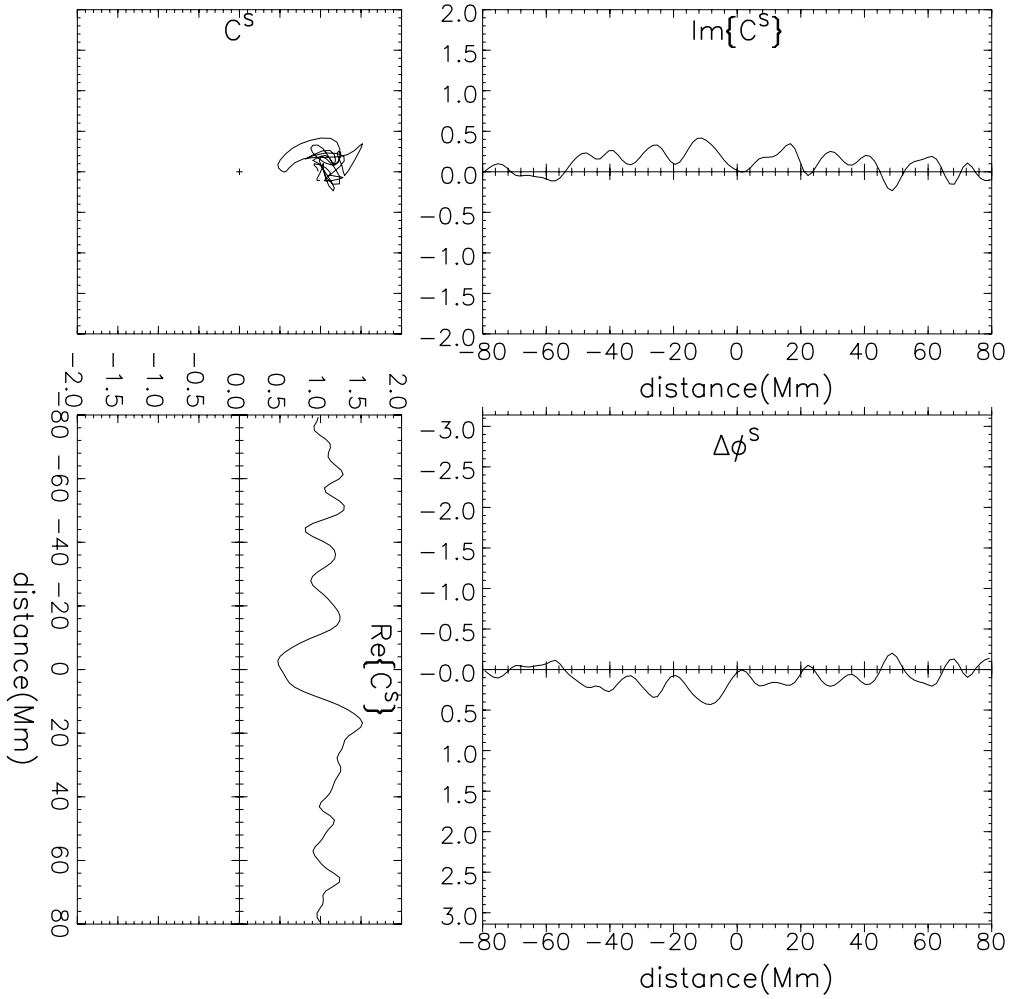

FIG. 8.—Diagnostic plots of the showerglass-corrected symmetric correlation, C^S, and symmetric phase, ϕ^S, from south to north through sunspot 2 at a depth of 7 Mm. The configuration for these is the same as for Fig. 3, with zero referenced to the center of sunspot 2 (see horizontal fiducial labeled "s2" in the right 7 Mm frame of Fig. 6).

sound-speed profile in the 0–3 Mm subphotosphere is uniformly 1.25 km s^{-1} greater than in the quiet subphotosphere within the cylinder. The increased sound speed results in a 40 s reduction in the one-way travel time through the sunspot photosphere. A very similar travel time reduction is likewise accomplished simply by removing the upper 340 km of the upper subphotosphere. The solid curve in Figure 12 is accordingly labeled "Photospheric Depression." This is roughly consistent with the acoustic Wilson depression derived on the basis of the local ingression control correlation, which was characterized in terms of a physical depression up to 450 Mm (see § 4.1 of Paper I). While we believe that a physical depression realistically contributes to both the large-scale diffuse signature and the local ingression control signature, we are convinced that the reality is more complicated. It probably involves an effectively increased sound some distance beneath the photosphere as well as other acoustic effects involving magnetic forces and thermal structure. We doubt whether a full 350–450 Mm depression of the sunspot photosphere would be accomplished by magnetic forces.

Kosovichev et al. (2000) propose a sunspot subphotosphere that is generally characterized by sound speeds in the range 0.5–1.0 km s^{-1} less than those of the quiet Sun in the 0–3 Mm subphotosphere and 0.5–1.0 km s^{-1} greater beneath 3 Mm, extending to depths of 10–12 Mm (see also Jensen 2003) or more in some cases. These tend to be confined to the volume directly beneath the sunspot with relatively little horizontal extension outside of the penumbral subphotosphere. The phase signature for such a model is plotted as a dashed curve in Figure 12 labeled "Cool ⊕ Hot." For the discussion that follows, we use the term "cool" to represent a region of reduced sound speed and "hot" to represent the region of enhanced sound speed. In the Cool ⊕ Hot model the sound speed is 0.5 km s^{-1} less than that of the quiet subphotosphere (Christensen-Dalsgaard et al. 1993) in the 0–3 Mm subphotosphere and 0.5 km s^{-1} greater to a depth of 10 Mm. The dotted curve shows arg C^S with only the cool, shallow anomaly present. The dot-dashed curve shows the same with only the hot, relatively deep anomaly present.

The measurements of ϕ^S cannot readily be fitted to anything approaching the Cool ⊕ Hot model or the individual components thereof. On the contrary, with the exception of measurements in the range 2–4 Mm, for which $|C^S|$ is dangerously near zero, the phase-correlation measurements strongly favor a sunspot subphotosphere in which the mean sound speed is, on the average, considerably increased over the 0–5 Mm range or, alternatively, a sunspot photosphere that is significantly depressed (*solid curve*).

The profile of a significant deep hot component by itself (*dot-dashed curve*) is readily distinguished from that of a shallow component of any temperature. The holographic model computations represented by the curves plotted in Figure 12 are relatively insensitive to the deep hot component with the focal plane at 4.2 Mm and about equally sensitive to both the deep hot

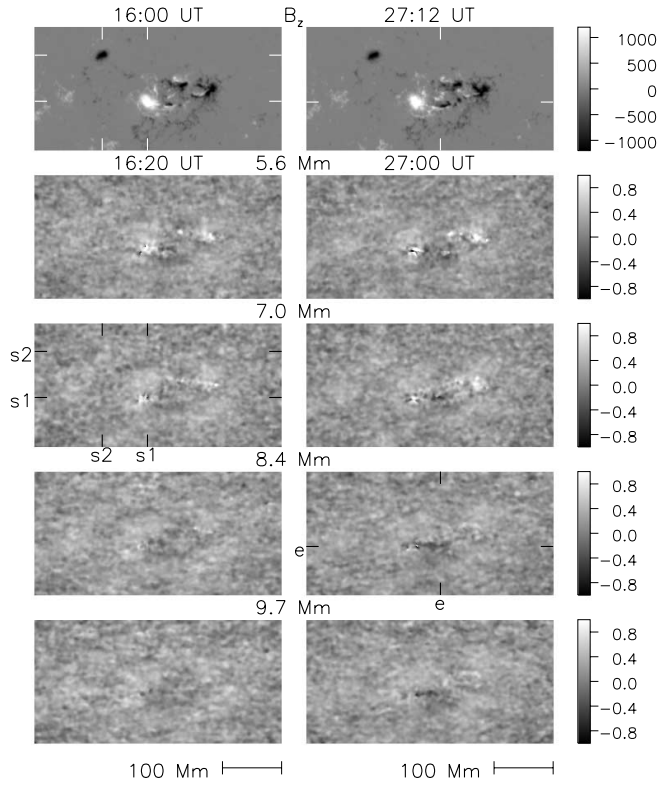

FIG. 9.—Gray-scale images of showerglass-corrected symmetric phase, ϕ^S, for AR 8179 for two consecutive 10.6 hr intervals. The left column shows ϕ^S integrated from 11:00–21:40 UT (i.e., 16:20 UT ±5 hr 20 minutes). The right column shows ϕ^S integrated from 21:40–08:20 UT the next day (i.e., 27:00 UT ±5 hr 20 minutes). Fiducials labeled "s1" and "s2" in the left 7 Mm frame locate sunspots 1 and 2. Fiducials labeled *e* in the right 8.4 Mm frame locate newly emerged magnetic flux in the interval 16:00–27:12 UT separating the magnetic observations.

and shallow cool components with the focal plane at about 10 Mm. Whether the mechanism of the travel time reduction is a heated layer or a physical depression, the phase-correlation measurements favor an anomaly that is predominantly shallow.

In principle, it is still possible to "hide" a cool 0–3 Mm layer in the 0–5 Mm subphotosphere. However, this would have to be overbalanced by hot material somewhere else in the 0–5 Mm subphotosphere or by an unwieldy Wilson depression. The introduction of hot material very much deeper than 5 Mm cannot offset the time delay caused by the cool layer in such a way as to satisfy the measurements.

Once again, it should be kept in mind that the model computations presented in Figure 12 are relatively crude, as they take no account of the suppression of the acoustic field in sunspot photospheres. While the foregoing results are strongly suggestive as to certain qualities of the active region subphotosphere, detailed three-dimensional computations of the MHD acoustics of shallow subphotospheric magnetic fields are needed to secure a realistic appraisal of the thermal structures of magnetic subphotospheres.

5.4. *Warm Anomalies Underlying Sunspots?*

Both the showerglass-corrected and uncorrected phase-correlation signatures presented in this study are consistent with subphotospheric anomalies that are relatively superficial. Most of the phase-correlation signature beneath 5 Mm appears to be predominantly due to an anomaly that is shallower than 5 Mm, one that could be compressed mostly into a range of a few hundred km as far as the phase-correlation signatures can currently discriminate. The predominance of the superficial anomaly is reinforced by the generally weak or absent holographic signatures of sunspot 2 at 7 Mm or deeper (see Fig. 6) when a phase correction based on the magnetic proxy is applied. These lead to a sound-speed anomaly averaged over the 3–10 Mm subphotosphere that is limited to the approximate range ±250 m s^{-1} if the horizontal extent of the anomaly is equivalent to that of the penumbra of sunspot 2. In the case of sunspot 2, a subphotospheric sound-speed enhancement of 0.5–1 km s^{-1}, such as that suggested by the models of Kosovichev et al. (2000), appears to be somewhat higher than the holographic signatures can comfortably accommodate if extended horizontally over the entire penumbral area of sunspot 2.

At this point, then, the showerglass-corrected phase-correlation maps are consistent with no sound-speed anomaly whatever underlying sunspots beneath 5 Mm. As before, we believe that detailed hydromechanical-acoustic computations applied to a flexible range of user-specified models are needed to securely resolve the question of whether the showerglass-corrected holographic computations, under certain conditions, can admit extended, warm subphotospheric anomalies such as those proposed by Kosovichev et al. (2000).

5.5. *The Large-Scale Diffuse Signature beneath* 5 Mm

While the large-scale diffuse component is greatly reduced by the showerglass correction, a significant component remains in Figure 9. At 7 Mm, for example, this signature is characterized by relatively positive phases on the eastern end of AR 8179 as compared to somewhat negative phases in the center of the region. That a signature of this scale would change as much as it does in 10.6 hr suggests that this is a manifestation of the proxy. This proposition is reinforced by the considerable strengthening of the diffuse signature in Figure 11 when the wrong magnetograms are applied to correct the showerglass. At this writing, the significance of a large-scale diffuse signature substantially beneath the showerglass must be regarded as negligible in terms of a submerged thermal anomaly.

5.6. *Compact Subphotospheric Anomalies Far from Sunspots*

Figure 9 shows signatures on a horizontal scale of 5–20 Mm at depths from 5.6 to 10 Mm, suggesting thermal variations up to 20%. An example is region *e*, shown in the right 8.4 Mm frame of Figure 9 and indicated by horizontal and vertical fiducials labeled accordingly. Based on various thermodynamic and mechanical considerations, such anomalies currently seem thoroughly unrealistic to us. The control comparisons shown in Figure 9 strongly suggest that signatures of this type are the result of surface magnetic evolution during the period over which the acoustic projections are integrated. This development suggests the need for a more accurate proxy, including more frequent magnetic observations to update the showerglass correction. Alternatively, a more flexible showerglass model that is not encumbered by limitations imposed by observations of the solar surface may be in order.

5.7. *Residual Showerglass Errors*

The basic exercise of Figure 9 was to contrive a showerglass correction that removes as much of the subphotospheric signature in ϕ^S as possible in the active region. Relatively little of the holographic signatures seen in Figure 1 remain beneath 5 Mm in Figure 9, after the showerglass correction has been applied. This limited control computation comfortably supports

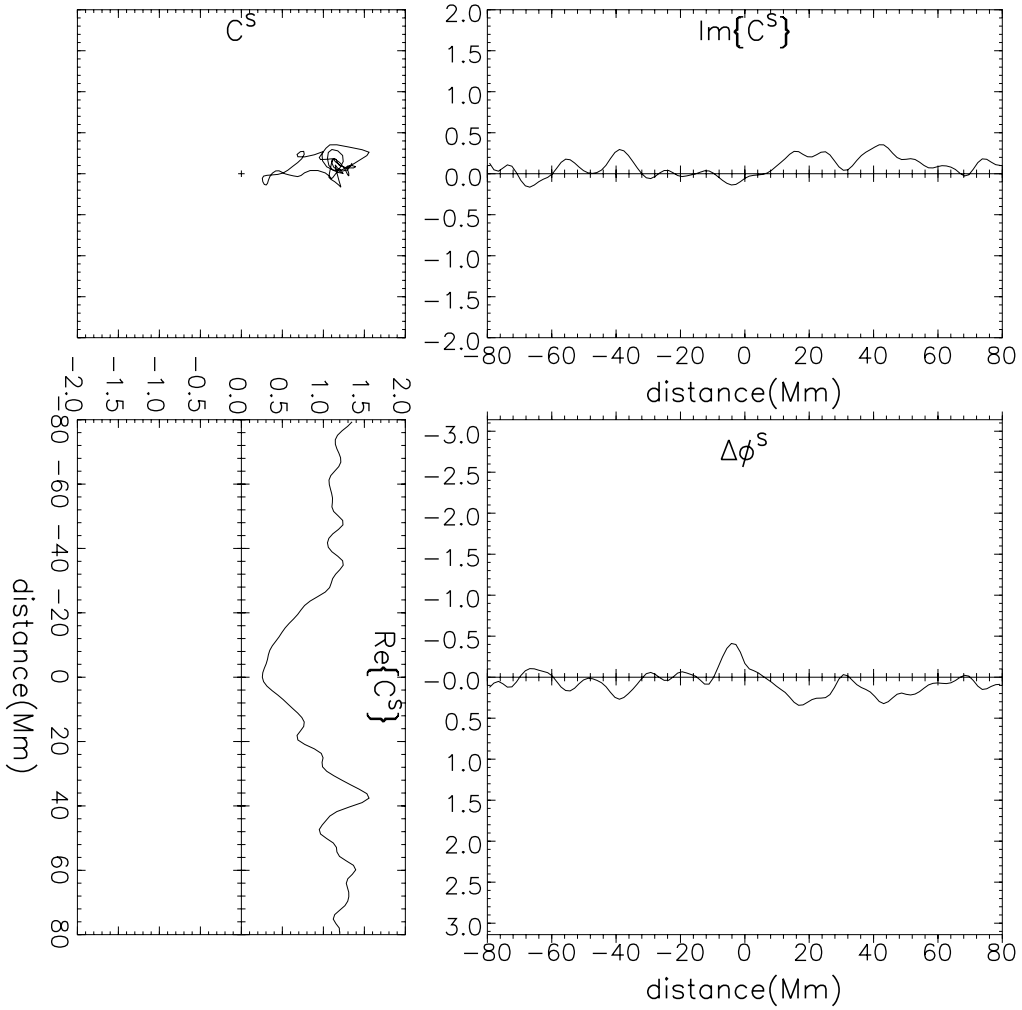

FIG. 10.—Diagnostic plots of the showerglass-corrected symmetric correlation, C^S, and symmetric phase, ϕ^S, from south to north through a region of emerging magnetic flux at a depth of 8.4 Mm. The configuration for these is the same as for Fig. 3, with the plot proceeding along the vertical fiducials labeled *e* in the right 8.4 Mm frame of Fig. 9 and referenced to zero passing between the horizontal fiducials labeled *e* in that frame.

the proposition that the substantially predominant component of the holographic signature of the active region subphotosphere beneath 5 Mm is the subphotospheric artifact projected by the showerglass. In fact, the magnetic proxy we developed for this study is quite crude. On one hand, it is rigid because of its dependence on a single magnetic parameter, B^2, under a potential-field assumption that is likely to be inaccurate. On the other hand, it does not adequately keep up with known changes in $\boldsymbol{B}$ during the interval over which the acoustic progressions are integrated. Yet again, the proxy does not include possible nonmagnetic contributors to the showerglass that could in principle be determined with some discrimination with standard modeling techniques. It is therefore evident that the signatures that remain in Figure 9 contain significant artifacts from residual showerglass errors.

6. WHAT IS NEEDED FOR REALISTIC SUBSHOWERGLASS DIAGNOSTICS?

6.1. *Basic Control Requirements*

Acoustic effects of thermal and magnetic anomalies are generally much greater at the surface than far beneath it. For example, a thermal anomaly at the surface, if submerged isentropically and conformally, is compressed into a much smaller volume with a smaller diameter and cross section area. The acoustic travel time through the submerged anomaly is decreased, not only because of the smaller diameter but because of a greater sound speed. The signature of the submerged anomaly in terms of a phase shift is reduced not only as a result of the smaller cross section but also because of more severe diffraction resulting from longer wavelengths due to the greater sound speed.

On the other hand, the signatures a superficial anomaly can project onto a submerged focal plane, while strong, are nevertheless limited in certain important respects. They must be relatively diffuse as a result of defocusing. They may be difficult to distinguish from the signatures of submerged anomalies that happen to be diffuse. However, a surface anomaly cannot consistently project a sharp artifact deep into the subphotosphere.

Because acoustic statistics are relatively poor, it is important to take advantage of alternative avenues to derive as much information as possible about acoustic conditions in the shallow subphotosphere. This is what a good magnetic proxy offers. Because of the systematic uncertainties in the magnetic proxy developed in this study, an important control consideration for the present is the question of to what extent the signatures that remain in Figures 6 and 9 could be artifacts projected by the remaining, uncorrected showerglass anomaly. Stated in the optical perspective, to what extent can the signatures that remain in Figures 6 and 9 be removed by adjusting the model of the showerglass to correct the phase perturbations it introduces at

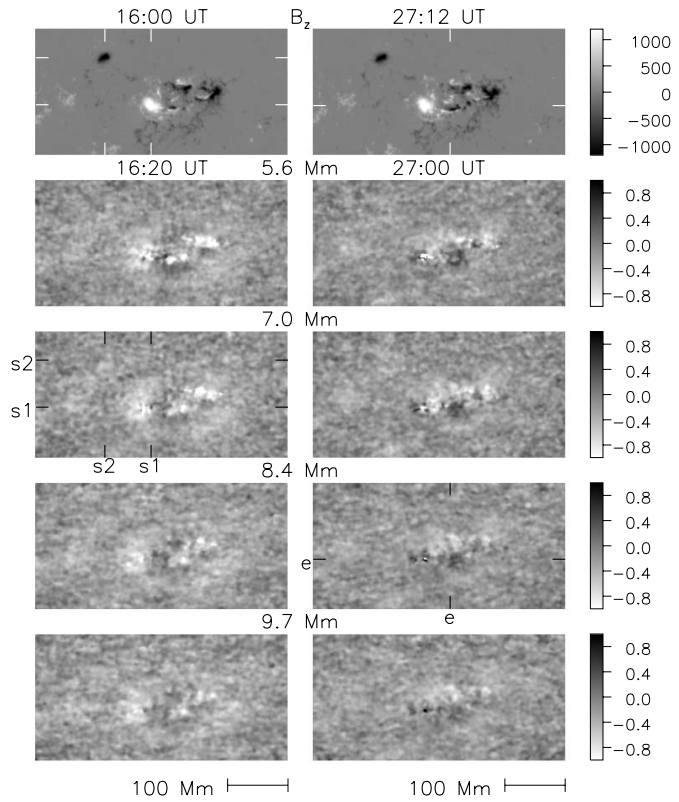

FIG. 11.—Computations represented in Fig. 9 are repeated with the magnetograms on which the showerglass correction was based swapped. Errors due to changes in the magnetic field over the interval 16:00–27:12 UT are substantial.

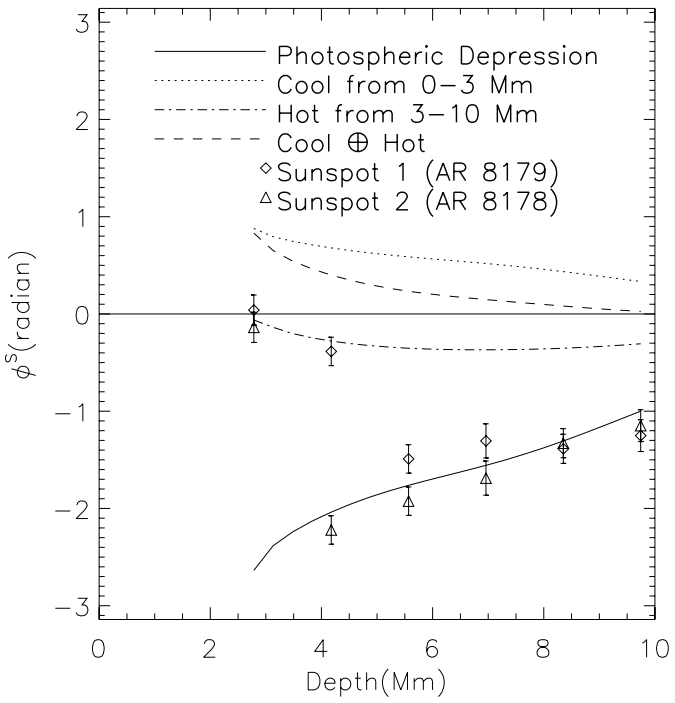

FIG. 12.—Symmetric phase signatures, ϕ^S, of sunspots, uncorrected for the showerglass, are compared with eikonal computations of the same for alternative sunspot models. The solid curve represents an acoustic Wilson depression, accomplished by removal of the upper 340 km of the photosphere over the penumbral area of sunspot 2. The dotted curve represents a 0–3 Mm subphotosphere of the same horizontal extent whose sound speed is 500 m s^{-1} less than that of the atmosphere of Christensen-Dalsgaard et al. (1993). The dot-dashed curve represents a 3–10 Mm subphotosphere of the same horizontal extent whose sound speed is 500 m s^{-1} greater than that of the atmosphere of Christensen-Dalsgaard et al. (1993). The dashed curve represents the composite of the models represented by the dotted and dot-dashed curves.

the solar surface? If it is possible, for example, to eliminate all significant holographic signatures that appear in the submerged phase maps by contriving an appropriate showerglass correction, then it must be regarded as dangerously likely that the original signatures are in fact artifacts projected into the subphotosphere by the showerglass in their entirety. Given the relatively large uncertainties that currently characterize the showerglass, for example, it is possible that the diffuse signatures that remain at 7 Mm in Figures 6 and 9 are the result of a diffuse anomaly 7 Mm beneath the solar surface. However, if these can be eliminated entirely by further, nonproxy adjustments in the showerglass model within realistic showerglass uncertainties, it would have to be considered likely that they are artifacts of the showerglass. It would require an exceptional accident for all of these signatures to be among the relatively few that could be removed in their entirety by a showerglass adjustment.

Therefore, the basic control work to address the proposition that submerged phase-correlation signatures are predominantly artifacts of the showerglass is to characterize as cleanly as possible the class of holographic signatures that can be projected by surface anomalies of any kind. The onus on the analyst is to exhaust the means whereby a relatively small anomaly at the surface can emulate the signature that the analyst proposes to attribute to a submerged anomaly within the uncertainties imposed by the showerglass.

6.2. *A More Flexible Showerglass Model*

The phase errors in the proxy we have developed illustrate the major liability of a proxy: systematic errors when the parameter basis of the proxy is incomplete. In fact, it is possible that the showerglass includes anomalies whose only consistent, reliable manifestation at the overlying surface is their helioseismic signature. In such a case, any proxy based on nonhelioseismic observations will be incomplete and limited accordingly. In principle, a practical showerglass correction can be accomplished without a proxy by standard modeling techniques that fashion the phase correction to optimize $|C^S|$ under appropriate constraints for appropriate submerged focal planes. The range of techniques for this purpose would be similar to that encompassed by standard techniques in adaptive optics. It is entirely worthwhile to apply these techniques in local helioseismology, free from constraints imposed by a proxy. In principle, if prospective appropriate corrections are examined exhaustively, the result can hardly be worse than that delivered by the best possible proxy.

6.3. *A Better Magnetic Proxy*

The simple magnetic proxy we have developed removes a substantial fraction of the phase error introduced by the acoustic showerglass in large active regions. However, it is evident that significant errors remain. The overwhelming advantage of a proxy is that it is based on observations that are encumbered with far smaller statistical uncertainties than helioseismic observations. Magnetic snapshots are generally much more accurate than acoustic measurements, even when the latter are integrated over many hours. In practice, then, there are solid grounds on which to anticipate that a well-designed proxy could, at the very least, expedite the search for the optimum showerglass correction.

Considerable progress toward an improved proxy is already being made in studies of the physics of the interaction between acoustic waves and photospheric magnetic fields. A remarkably

interesting aspect of this interaction has to do with the difference between the local control correlations $C_{\rm LC-}$ and $C_{\rm LC+}$ (see § 2.2 of Paper I), particularly the difference in phase, discovered by Duvall et al. (1996). Braun (1997) suggested a range of dynamical factors based on relatively superficial anomalies to explain the phase asymmetry. We now think that the difference between $C_{\rm LC+}$ and $C_{\rm LC-}$ in strong magnetic fields would have to be, in significant part if not entirely, the signature of time-irreversible acoustic qualities of the direct interaction between upcoming acoustic waves and the photospheric magnetic field, qualities that are also responsible for a strong absorption of acoustic waves by magnetic regions. We have already cited considerations relating the coupling of compression waves to slow Alfvén waves (Cally 2000; Crouch & Cally 2003), which provide that substantially inclined magnetic fields, $\boldsymbol{B}$, significantly shift the phases of the photospheric Doppler signatures of vertically ascending acoustic waves. When the acoustic observations, ψ, are line-of-sight Doppler maps, the phase of $C_{\rm LC-}$ is significantly dependent not just on the tilt of the magnetic field but also on the inclination of the line of sight and its azimuth with respect to that of the horizontal component, $B_\perp$, of the field, $\boldsymbol{B}$. The theory being developed by Cally (2000) and Crouch & Cally (2003) therefore promises to open the door to a greatly improved magnetic proxy.

6.4. *Better Helioseismic Observations?*

We understand that the Helioseismic Magnetic Imager (HMI) on the *Solar Dynamics Observatory* (*SDO*) is designed to obtain observations of sunspot umbrae considerably superior to the MDI observations. This will certainly be useful for diagnostics of sunspot subphotospheres. At the same time, we reiterate the conclusion of Paper I (see their § 4.4), based on MDI measurements of the "local ingression control correlations," that the MDI Doppler acoustic signatures in sunspot umbrae, while substantially noisier than those of the quiet Sun, nevertheless appear to be considerably more substantial than is generally realized.

6.5. *Broader Spectral Coverage*

In this study, we have examined only the higher frequencies, based on the possibility that the showerglass could be largely corrected in a way that the effects of diffraction and relatively poor statistics cannot. We are now preparing to repeat this exercise as a control exercise in the 3 mHz spectrum. The phase errors introduced by the showerglass at 3 mHz are substantially smaller than those at 5 mHz, roughly in proportion to frequency. The signals to be expected are smaller and the diffraction effects more severe in roughly similar proportion. However, sound-speed anomalies such as those that appear in the models of Kosovichev et al. (2000) should give rise to significant holographic signatures in the 3 mHz spectrum if integrated over a reasonable time.

6.6. *Simulated Sound Computations*

What is now most particularly needed in practical terms of control work is the facility to run accurate computational progressions of acoustic noise propagating through realistic models of local refractive anomalies and flows that could prospectively represent active region subphotospheres. These computations should include a careful account of the interaction of acoustic waves with submerged magnetic, thermal, and Doppler anomalies as well as with the acoustic showerglass itself.

The foregoing proposition is similar in certain respects to that on which computational seismic holography is founded. In fact, the difference is critical. Holography proposes to acoustically project waves observed at the surface into the solar interior, both forward and backward in time, but under the assumption that the solar interior medium contains no intervening local acoustic anomalies between the surface and the focal plane. Now needed are detailed hydromechanical computations of how acoustic waves interact with realistic subphotospheric anomalies and how their signatures at the solar surface are changed by the interaction. Simulated sound computations will give us a flexible and powerful control tool to reinforce modeling of the showerglass itself. This particularly applies to ongoing holographic modeling of the penumbral phase anomaly and the contribution of ghost signatures in the islands of anomalous phase that appear in phase-correlation maps over shallow focal planes. In our opinion, simulated sound computations have now become the major diagnostic tool needed in local helioseismology for purposes of forward modeling of compact anomalies in the shallow subphotosphere.

7. SUMMARY

Correlation statistics between holographic projections and local acoustic and magnetic fields in active regions in the 4.5–5.5 mHz spectrum show signatures suggesting a strong, superficial acoustic anomaly directly beneath active regions. It is evident that the shallow magnetic subphotosphere can introduce phase shifts up to 90° into acoustic waves impinging into the photosphere from the underlying solar interior. These phase shifts can significantly impair the coherence of acoustic emission from submerged sources or scatterers, degrading phase-correlation statistics and images of subphotospheric anomalies computed by phase-coherent acoustic reconstruction. Because of this, we refer to this anomaly as the "acoustic showerglass."

In an independent study (Paper I) we characterized the acoustic showerglass in terms of the "local control correlations," $C_{\rm LC+} = \langle H_+ \psi^* \rangle$ and $C_{\rm LC-} = \langle \psi H_-^* \rangle$, between subjacent acoustic progressions, $H_\pm$, to a surface focal point, $\boldsymbol{r}$, from a distant pupil, and the local acoustic field, ψ, at $\boldsymbol{r}$. We used these measurements to devise a magnetic proxy for phase and amplitude perturbations introduced by the showerglass and apply the proxy to helioseismic observations to correct the perturbations. In this study we have applied phase-correlation holography in the lateral vantage to helioseismic observations of an active region over the 4.5–5.5 mHz spectrum with and without corrections for the showerglass. In particular, we study maps of the phase, ϕ^S, of the "symmetric ingression-egression correlation," C^S, over focal planes ranging from 5 to 10 Mm in depth.

For helioseismic observations of an active region uncorrected for the showerglass, the predominant subphotospheric signature in the ϕ^S subphotosphere appears to be a relatively diffuse component characterized by a significantly advanced phase, equivalent to travel time reductions of 50–100 s. This appears to be an artifact projected by the showerglass itself. The phase signature of a moderately large sunspot is approximately reproduced by a model in which the upper 350 Mm of the subphotosphere over the penumbra and umbra has simply been removed. While the reality is clearly more complicated than just a photospheric depression, this is roughly consistent with the acoustic Wilson depression that reproduces the local ingression control signatures measured in Paper I.

Maps of ϕ^S for a large active region are punctuated by sharply defined islands of somewhat stochastic phase with a tendency to be retarded in the shallow focal planes. These are regions in which the phase correlation, C^S, has collapsed, attributed partly to suppression of the acoustic signature in

strong magnetic photospheres and partly to the impairment of the correlation by the phase perturbations introduced by the showerglass. In active regions, the islands may also be susceptible to "ghost signatures," which represent interference from waves traveling in the "wrong" direction.

For helioseismic observations of the active region that have been corrected for the showerglass, maps of ϕ^S show some residual features down to a depth of 10 Mm. However, these appear to be artifacts of showerglass perturbations that have escaped the phase correction. Based on signatures shown by control computations to render a rough appraisal of uncertainties remaining after the showerglass correction, we currently see no evidence of significant sound-speed anomalies beneath 5 Mm.

A better understanding of the interaction of acoustic waves with photospheric and shallow subphotospheric magnetic fields could give us a magnetic proxy considerably superior to that applied in this study. A magnetic proxy for helioseismic imaging of sunspot subphotospheres could benefit considerably from Stokes magnetic observations the HMI will give us from the *SDO*. Cleaner acoustic observations of sunspot umbrae will likewise be very welcome. What is now most particularly needed in practical terms for models of local subphotospheric refractors and flows is the facility to run detailed hydromechanical computations of acoustic noise propagating through user-specified local acoustic anomalies over the spectrum encompassing known solar interior acoustics. Simulated sound computations, properly formulated and applied to realistic models of prospective acoustic anomalies, will provide a powerful diagnostic tool for control purposes accessible to any diagnostic technique that can be applied to actual helioseismic observations. Simulated sound computations currently being planned will include a careful account of the interaction of acoustic waves with submerged magnetic, thermal, and Doppler anomalies as well as with the showerglass itself. In our opinion, credible simulated sound computations have become the crux of a clear understanding of the subphotospheres of active regions. We now regard this requirement as fundamental in terms of control work in local helioseismology of active region subphotospheres.

We greatly appreciate consultation with P. S. Cally and H. Schunker at Monash University regarding their work on the acoustics of shallow subphotospheric magnetic fields. We also thank the referee, Tom Duvall, for his careful study of the paper and his thoughful comments. This research was supported by grants from the Stellar Astronomy and Astrophysics Program of the National Science Foundation and the Sun-Earth Connection/Living With a Star and Supporting Research and Technology programs of the National Aeronautics and Space Administration.

REFERENCES

Braun, D. C. 1995, ApJ, 451, 859
———. 1997, ApJ, 487, 447
Braun, D. C., Duvall, T. L., Jr., LaBonte, B. J., Jefferies, S. M., Harvey, J. W., & Pomerantz, M. A. 1992a, ApJ, 391, L113
Braun, D. C., & Lindsey, C. 2000, Sol. Phys., 192, 307
Braun, D. C., Lindsey, C., Fan, Y., & Jefferies, S. 1992b, ApJ, 392, 739
Cally, P. S. 2000, Sol. Phys., 192, 395
Christensen-Dalsgaard, J., Proffitt, C. R., & Thompson, M. J. 1993, ApJ, 403, L75
Crouch, A. D., & Cally, P. S. 2003, Sol. Phys., 214, 201
Duvall, T. L., Jr., D'Silva, S., Jefferies, S. M., Harvey, J. W., & Schou, J. 1996, Nature, 379, 235
Fan, Y., Braun, D. C., & Chou, D.-Y. 1995, ApJ, 451, 877
Hindman, B. W., Haber, D. A., Toomre, J., & Bogart, R. 2000, Sol. Phys., 192, 363
Jensen, J. M. 2003, in Local and Global Helioseismology: The Present and Future, ed. H. Sawaya-Lacoste (Noordwijk: ESA), 61
Kosovichev, A. G. 1996, ApJ, 461, L55
Kosovichev, A. G., Duvall, T. L., Jr., & Scherrer, P. H. 2000, Sol. Phys., 192, 159
Lindsey, C., & Braun, D. C. 2000, Sol. Phys., 192, 261
———. 2004, ApJS, 155, 209 (LB04)
———. 2005, ApJ, 620, 1107 (Paper I)